()

Full multiple scattering analysis of XANES at the Cd L_3 and O K edges in CdO films combined with a soft-x-ray emission investigation

I. N. Demchenko,[1,2,3] J. D. Denlinger,[2] M. Chernyshova,[4] K. M. Yu,[2] D. T. Speaks,[2,5] P. Olalde-Velasco,[2,6] O. Hemmers,[1] W. Walukiewicz,[2] A. Derkachova,[3] and K. Lawniczak-Jablonska[3]

[1]*Department of Chemistry, University of Nevada–Las Vegas, 4505 Maryland Parkway, P.O. Box 454003, Las Vegas, Nevada 89154-4003, USA*

[2]*Lawrence Berkeley National Laboratory, 1 Cyclotron Rd., Berkeley, California 94720-8235, USA*

[3]*Institute of Physics PAS, al. Lotnikow 32/46, 02-668 Warsaw, Poland*

[4]*Institute of Plasma Physics and Laser Microfusion, 23 Hery Street, 01-497 Warsaw, Poland*

[5]*Department of Materials Science and Engineering, University of California, Berkeley, California 94720, USA*

[6]*Instituto de Ciencias Nucleares, UNAM, Mexico, Distrito Federal 04510, Mexico*

(Received 19 March 2010; revised manuscript received 5 July 2010; published 5 August 2010)

X-ray absorption near edge structure (XANES) at the cadmium L_3 and oxygen K edges for CdO thin films grown by pulsed laser deposition method, is interpreted within the real-space multiple scattering formalism, FEFF code. The features in the experimental spectra are well reproduced by calculations for a cluster of about six and ten coordination shells around the absorber for L_3 edge of Cd and K edge of O, respectively. The calculated projected electronic density of states is found to be in good agreement with unoccupied electronic states in experimental data and allows to conclude that the orbital character of the lowest energy of the conductive band is Cd $5s$-O $2p\sigma^*$. The charge transfer has been quantified and not purely ionic bonding has been found. Combined XANES and resonant inelastic x-ray scattering measurements allow us to determine the direct and indirect band gap of investigated CdO films to be $\sim$2.4 eV and $\sim$0.9 eV, respectively.

()

I. INTRODUCTION

The interest on transparent conducting oxides (TCOs) has never diminished since it was originated in the middle of the 1960s. In recent years TCOs have attracted considerable attentions due to their tremendous importance in applications such as displays, photovoltaic cells, touchscreens, electrochromic windows, etc. The number of known TCOs is not large and most of them (such as ITO and ZnO) have been studied extensively. In comparison, much less effort has been devoted to cadmium oxide CdO, a material belonging to II-VI group of compounds whose properties differ from commonly used and well-known indium (In_2O_3) and tin (SnO_2) oxides. Typically it was found that as-grown CdO films are highly n-type with an electron concentration higher than $10^{19}/cm^3$.[1] This is believed to be due to the pinning of the Fermi energy at $\sim$1.15 eV above the conduction band edge (E_C) on the free CdO surface.[2] It is similar to the situation observed in the well-known narrow gap InN materials.[3] The high free electron concentration of CdO materials also results in a blueshift in the optical absorption edge due to the Burstein-Moss effect.[4–6]

The controlled synthesis of CdO structures and in-depth understanding of their chemical/physical properties versus electronic structure are the key issues for the future development of CdO-based devices. The electronic structure of CdO studied by x-ray techniques has been reported by several authors. McGuinness *et al.*[7] used x-ray absorption (XAS) and emission (XES) spectroscopies to study the influence of shallow core-level hybridization on electronic structure of the post-transition-metal oxides (including polycrystalline CdO). In another paper by Dou *et al.*,[8] polycrystalline ceramics samples of CdO doped by Y and In were probed using photoemission spectroscopy. They observed a shift to higher binding energy of core levels and valence band (VB) features for doped CdO material. Since this shift was less than the change in the width of the occupied conduction band (CB) the authors proposed to use it as a direct measurement of band gap shrinkage as a result of doping. Recently, Piper *et al.*[9] reported a soft x-ray emission and absorption investigation on the electronic structure of single-crystal rocksalt CdO samples. These authors also compared the experimental data with *ab initio* band structure calculations obtained from the hybrid density-functional-theory (DFT) computations using HSE03 functional for exchange and correlation with taken into account quasiparticle effects by GW (Ref. 10) corrections of the HSE03 eigenvalues. Presented resonant XES data reveal clear Cd $4d$-O $2p$ hybridized peak and momentum-dependent coherent contributions to the resonant emission spectra. Using high-resolution x-ray photoelectron spectroscopy (XPS) measurements, King *et al.*[11] probed the VB structure of single crystal CdO and compared their experimental results with DFT theory calculations incorporating quasiparticle effects. These prior studies have succeeded in obtaining some basic understanding of the electronic structures of CdO. However, the fundamental issues such as band gaps size of CdO are still controversial. In this paper, we present XAS and XES/RIXS measurements on CdO that will address on some of these fundamental issues. XAS and XES directly probe the partial density of states (DOS) of the CB and VB, respectively. Overlapping the XES and XAS spectra with reference to the core level provides a direct measurement of the energy positions of the VB and CB states in semiconductor materials which cannot be derived from optical measurements. The experimental XANES data were compared to results of *ab initio* calculations done by

FEFF code.[12,13] This code has the real-space Green's function approach as a base [also called the real-space multiple scattering (RSMS) approach]. It is essentially a quasiparticle approximation that takes into account final state effects, including inelastic losses, core-hole effects, lifetime, and Debye-Waller factors.

This paper aims to develop a comprehensive understanding of the electronic properties of a significantly cation-anion mismatched semiconductor, CdO, focusing specially on the occupied and unoccupied band edges behavior. This is motivated by the dual goals of furthering the knowledge and understanding of their material properties for potential use in device applications, and the investigation of novel physical phenomena in solid state physics.

II. EXPERIMENTAL AND DATA ANALYSIS

The CdO films (marked as "*A*" and "*B*") were deposited by pulsed laser deposition on *c*-plane sapphire substrates. A Lambda Physik KrF excimer pulsed laser operating at 248 nm with a pulse width of 10 ns, energy fluence of 160 mJ and repetition rate of 5 Hz was used. Sapphire substrates, 6 mm by 6 mm, were first cleaned with acetone followed by methanol. After mounting in the chamber, the substrates were baked at 500 °C for 30 min to remove any residual contamination. A distance of 6 cm was maintained between the substrate and the pure Cd target during deposition. The two films were deposited at 310 °C and 242 °C, respectively with 40 000 laser pulses. Prior to deposition, the chamber was pumped down to 1×10^{-6} torr. During deposition the background pressure was maintained at a constant 4.2×10^{-4} torr by flowing O_2.

The crystal structure of the investigated films was determined by x-ray diffraction (XRD) method using a Siemens D700 diffractometer. The incidence radiation was Cu $K\alpha$ (at 40 kV and 30 mA). The films thickness (*A*: 240 and *B*: 188 nm) was measured by Rutherford backscattering spectrometry (RBS) using a 2 MeV He^+ ion beam with a Si surface barrier detector positioned at 165° with respect to the incident beam. The optical absorption edges were measured using a Perkin-Elmer Lambda 950 Spectrophotometer (190–3000 nm) at room temperature. Electron concentrations and mobilities were determined by Hall Effect in the Van der Paaw configuration using an Ecopia HMS-3000 system with a 0.6 T magnetic field.

The investigations of the cadmium L_3 and oxygen K edges were performed by x-ray absorption and emission measurements at room temperature on the 9.3.1 and 8.0.1 beamlines (BLs) at the Advanced Light Source (ALS, Berkeley, USA). XANES spectra were gathered with an energy resolution of about 0.4 and 0.2 eV (BL 9.3.1 and 8.0.1, respectively) in the total fluorescence yield (TFY) detection mode. TFY detection is more bulk sensitive and is preferable in our case since the following x-ray emission measurements are also bulk sensitive. Since the CdO films are thin compared to two absorption lengths, self-absorption effect is negligible for both edges. TFY data were collected using a Hamamatsu Si photodiode or a negatively biased channeltron (on 9.3.1 and 8.0.1 BLs, respectively). The size of incident beam was about $4\times0.5(0.2)$ mm. Soft XES and RIXS on 8.0.1 BL were measured using the Tennessee/Tulane grating spectrometer with a total energy resolution of 0.6 eV. XES energy values were aligned with the XAS photon energy scale by using the elastic emission as a marker for the excitation energy. All of the presented XANES spectra are averaged through at least two data sets, where a pre-edge linear background was subtracted and the edge step was normalized to unity.

XANES spectra were calculated using the *ab initio* code FEFF8 within the real-space full multiple-scattering (FMS) approach.[12,14] This code implements the single-electron theory, based on a self-consistent real-space Green's function formalism and final-state potentials taking into account an appropriately screened core hole. For better understanding of the further interpretation of experimental XANES spectra in terms of RSMS formalism we would like to mention some known aspects. In short, the probability of the dipole mediated transition of a deep core electron for XAS is described, by Fermi's Golden Rule

$$\mu_a \propto \sum_{f}^{E_f\rangle E_F} |\langle f|\hat{E}\cdot r|i\rangle|^2 \delta(E-E_f), \tag{1}$$

where $|i\rangle$ corresponds to electron initial state of the absorbing atom "*a*," $|f\rangle$—some unoccupied state, $\hat{E}\cdot r$ is the dipole operator for the incidence beam interacting with the material, and the sum is over all energies above the Fermi energy. Deep-core states in this work are $2p$-Cd and $1s$-O. Skipping the details, which can be found in Refs. 13–15, Eq. (1) can be rewritten (using scattering theory) in terms of the photoelectron Green's function or propagator

$$\mu_a \propto -\frac{1}{\pi}\mathrm{Im}|\langle i|\hat{\mathrm{E}}^*\cdot rG(E)\hat{\mathrm{E}}\cdot r|i\rangle|\Theta(E-E_F), \tag{2}$$

where, Θ is a broadened step function ensuring that the cross section is nonzero only above the Fermi energy, E_F. G is the full, one-electron propagator in the presence of the scattering potential and is expressed by the Dyson equation $G=G^0+G^0TG^0$, where G^0 is the free electron propagator and T is the full, atomic scattering matrix.[16,17] Solving the Dyson equation with T expressed in terms of the single site scattering matrices, t, it is obtained as a Taylor expansion

$$G = G^0 + G^0tG^0 + G^0tG^0tG^0 + \cdots, \tag{3}$$

$$G = (1-G^0t)^{-1}G^0. \tag{4}$$

In another words, after the photo ionization process the ejected photoelectron can be described as a spherical wave which propagates outwardly from the absorber. The G propagator describes all possible paths (ways) that the photoelectron can scatter from one or more of the neighboring atoms before the core hole is refilled. Propagation of the electron between two points in space is determined by the free electron propagator, G^0. Finally, t describes how a photoelectron scatters from a single atom. The significant result of the multiple-scattering formalism is that the expression for the absorption cross section $\mu_a(\varepsilon)$ can be factored in terms of an atomic background absorption, $\mu_0(\varepsilon)$, modulated by the mul-

TABLE I. Structure of ten coordination shells cluster for CdO, based on the lattice parameter a =4.693 Å (from our XRD measurements).

Coordination shell number	Neighboring atom		Number of atoms in the coordination shell	Coordination shell radius (Å)
	Around O	Around Cd		
1	Cd	O	6	2.34650
2	O	Cd	12	3.31845
3	Cd	O	8	4.06426
4	O	Cd	6	4.69300
5	Cd	O	24	5.24693
6	O	Cd	24	5.74773
7	O	Cd	12	6.63690
8	Cd	O	30	7.03950
9	O	Cd	24	7.42028
10	Cd	O	24	7.78246

tiple scattering fine structure function, $\chi_l(\varepsilon)$, where l is the final state angular momentum and ε is the relative energy ($\varepsilon=E-E_0$, E is absolute energy and E_0 is absorption edge energy)

$$\mu_a(\varepsilon) = \mu_0(\varepsilon)[1 + \chi_l(\varepsilon)]. \quad (5)$$

To compute XANES spectra Eq. (4) is solved directly by explicitly inverting the matrix $(1-G^0t)$ while to analyze the extended x-ray absorption fine structure (EXAFS) region a sum over scattering paths of expanded Eq. (3), cleverly truncated, is used as the basis.

Equation (3) contains all orders of scattering. Thus G^0tG^0 describes all possible ways of electron scattering of only one neighboring atom. $G^0tG^0tG^0$ describes all the ways that a photoelectron can scatter from exactly two surrounding atoms. The next term in the series describes all the ways that a photoelectron can scatter exactly three times, and so on. So, each term in Eq. (3) can be further expanded as a sum over all specified paths of a given order. This is the so called MS formalism (see results for L_3 edge of Cd).

Let us underline, that Eq. (4), being a convolute version of Eq. (3), contains the contributions from all orders of scattering. Inverting the matrix $(1-G^0t)$ and multiplying by the G^0 matrix is used in the so called FMS. It is definite, that the FMS module sums all MS paths within the specified cluster. If the FMS card is not presented in the *feff* input file, MS path expansion is used; more details are presented elsewhere (Ref. 18).

The FMS calculations of the cadmium L_3- and oxygen K-edges XANES were performed for different cluster sizes (specified as spheres of a given radius around the absorbing atom) of CdO which has the rocksalt structure ($Fm3m$ space group) with the lattice parameter a=4.693 Å and coordination shells presented in Table I (type of atoms around the absorbing one; number of atoms; shell radii). The coordinates of atoms in each cluster are taken from the crystal structure of CdO compound.

The best results were obtained using the Hedin-Lundqvist self-energy together with additional energy shift (EXCHANGE card), $V_r \approx 1.83$ eV (K edge of O) and about 1.7 eV (L_3 edge of Cd) in order to set the Fermi level. The self-consistency was achieved for cluster size of about 5 Å (the SCF card) corresponding to 33 atoms including the absorber. In the final analysis the FMS was used (the FMS card) for a cluster of radius 8 Å surrounding the absorber (171 atoms for CdO). To perform the potentials and FMS calculations the angular-momentum cutoffs of the basis (l_scmt and l_fms) were increased for +1 with respect to atomic configuration and set to 3 for Cd and 2 for O (the POTENTIALS card). This guarantees that the program does not miss possible, due to hybridization, higher (partially) occupied l states. Lorentzian broadening with HWHH (half-width at half-height) equal to 0.1 eV was used for calculated spectra. All muffin-tin spheres were automatically overlapped by 15% (AFOLP card) to reduce the effects of potential discontinuities at the muffin tins. The XANES spectra were calculated in the presence of an appropriately screened core hole according to the final-state rule. The results of the calculations are shown in Figs. 1(b)–1(d), 2(b), and 2(c). The angular-momentum-projected local density of states (PDOS) is calculated for each distinguishable atom in the system (local DOS card). This is done using the FMS card. So, FMS fine structure functions, $\chi_{l,i}(\varepsilon)$, are computed from full one-electron propagator, G, and used to obtain new electronic densities of state for each atomic species i in the ensemble and for each angular momentum state l, as given by Ankudinov *et al.*[12] $\rho_{l,i}(\varepsilon)=\rho^0_{l,i}(\varepsilon)[1+\chi_{l,i}(\varepsilon)]$. The new electronic configurations are used to recompute photoelectron scattering amplitudes and phases for each atom in the ensemble and, in turn, are used to recompute the $\chi_{l,i}(\varepsilon)$ functions. This process is iterated in the loop until the $\chi_{l,i}(\varepsilon)$ functions have converged.

III. RESULTS AND DISCUSSION

Cadmium oxide is the only compound with NaCl structure among the cadmium chalcogenides. The XRD studies indicate that our films have cubic structure with well defined two peaks with orientation in the (200) and (400) planes. Observed lattice spacing "d" values are in good agreement

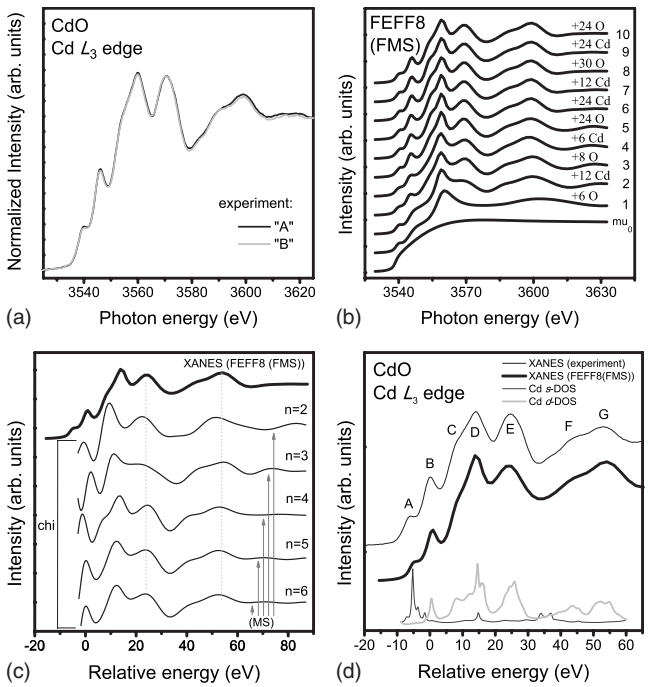

FIG. 1. (a) L_3 edge of Cd experimental XANES spectra for CdO layers (with different thickness and growth temperature) gathered in TFY detection mode. (b) Effect of increasing the number of scattering shells for the FMS calculation of the cadmium L_3 edge of CdO film (see text for details). (c) Comparison between theoretical XANES (upper thick curve, FMS) and EXAFS (thin curves, MS) for CdO. The theoretical EXAFS signals χ_n (chi) were calculated for ten shells cluster within MS formalism up to n order. (d) Theoretical XANES spectrum (thick line) with s and d DOS of Cd (dark and light gray lines, respectively) versus experimental XANES spectrum (thin line). E_F energy is −5.554 eV by FEFF8 code calculations. During calculation the Fermi level was shifted down (to place it in the midgap) by $V_r \approx 1.7$ eV (see text). In (b)–(d) the data were vertically offset.

with standard "interplanar spacing, d" values. Hall effect measurements of these films show that they are n-type with electron concentration and mobility in the range of $8-10 \times 10^{19}/\mathrm{cm}^3$ and $\sim 100\ \mathrm{cm}^2/\mathrm{V\,sec}$, respectively. We note that our CdO films are rather of high quality since the electron mobility is quite high for such electron concentration.

The atomic orbital configuration of Cd is $4d^{10}5s^2$ and O-$1s^2 2s^2 2p^4$. In principle, the chemical bonds for this metal oxide may have an appreciable degree of ionic character and the outermost electron configuration of Cd^{2+} and O^{2-} ions is $4d^{10}$ and $2p^6$, respectively. Also, it may have a purely neutral configuration or mixing of these chemical bondings with predominance of one of them. For purely ionic or neutral character of bonding in CdO, O $1s \rightarrow 2p$ or Cd $2p \rightarrow 5s$ transitions, respectively, should not be observed.

Cadmium and oxygen absorption edges provide complementary information. The oxygen K-edge XANES extends up to about 25 eV above the Fermi level covering a small part of the energy range available at the cadmium L_3 edge which goes up to 70 eV. However, the energy resolution at the O K edge is significantly better due to much smaller natural core-hole level width (0.16 eV of Ref. 19) in comparison with the Cd L_3 edge (2.50 eV of Ref. 20). Besides, these XANES signals allow probing unoccupied states with different orbital momentum.

A. Cadmium L_3 edge—XAS

According to the dipole selection rule, for cadmium L_3 edge, only transitions from atomiclike Cd $2p_{3/2}$ state to unoccupied states with s and d character above the Fermi level are allowed. The normalized experimental Cd L_3 edge XANES spectra are shown in Fig. 1(a). No difference in the XANES shape profile, threshold, and peak positions was observed for both CdO films. This is in agreement with the results of our XRD, RBS, and Hall measurements that show that the two films are very similar. The Cd L_3-edge XANES spectra are directly compared to spectra calculated using the ideal NaCl structure (octahedral symmetry) by FEFF8 code. One of the important tasks in any FEFF calculation is to ensure that the results converge with respect to the size of FMS cluster. In Fig. 1(b) we show the results of the FMS calculations with increasing ensemble size (calculations were done with successive supplement of the next coordination shell around the central Cd atom to the previous cluster). The number of coordination shells around the absorber varies from 1 to 10. Here, μ_o (mu_0) is pure atomic absorption, i.e., in the absence of neighboring atoms, which does not manifest any structure. Convergence in terms of peaks number (and their positions) in the fine structure appears to be reached after inclusion of six coordination shells (as indicated in Table I). Adding the next coordination shells does not change the fine structure (except some weak details which could only be verified by using high-resolution XANES data). Comparing experimental spectra with PDOS calculations one notices that the main peaks can be attributed to the final state with Cd $5d$ character, which are split by the octahedral crystal field of oxygen atoms. The small pre-edge feature A [Fig. 1(d)] corresponds to transition from Cd $2p_{3/2}$ to antibonding a_{1g}^* molecular orbital determined mainly by metal $5s$ orbitals. In terms of the MS theory, the peak D [Fig. 1(b) and 1(d)] arises already when six oxygen atoms, located in the first coordination shell, are included into calculation and it is not changed significantly upon further increase in the cluster size. Many scattering interferences appear when two more coordination shells are added. When the next-nearest 12 Cd atoms are added, features E, F, and G start to reveal. The final shape of post-threshold region in the XANES spectrum for scatterings around the absorber is reached when additional eight atoms of oxygen in the next shell are considered in the calculation. Further increasing cluster size influences mainly on threshold profile modification, thus, makes the pre-edge peak B, detected in the experimental spectrum, well resolved on the theoretical XANES curve when five coordination shells FMS is performed.

The origin of the F-G peaks around 35–70 eV is specified in Fig. 1(c). These peaks are attributed to the interference effects between different MS signals and represent the beginning of EXAFS region. We present here a comparison of several EXAFS signals χ_n, calculated within MS formalism up to the n order with the theoretical XANES calculated

within FMS formalism. The smallest cluster size, where the multiple photoelectron scattering is able to reproduce these peaks with quite good visibility, is about six coordination shells around the absorbing cadmium atom. Further increase in the cluster size to ten shells does not result in any new features but only slightly improves the resolution of the peaks. Here, $\chi(n=2)$ corresponds to the sum of all single-scattering (SS) signals [i.e., Cd$\rightarrow$O(first shell)$\rightarrow$Cd; Cd $\rightarrow$Cd$'$(second shell)$\rightarrow$Cd; and so on], $\chi(n=3)$ denotes the sum of all SS and double-scattering (DS, for instance: Cd $\rightarrow$O$\rightarrow$Cd$'\rightarrow$Cd; Cd$\rightarrow$O$\rightarrow$O$'\rightarrow$Cd; and so on) signals, $\chi(n=4)$ denotes the sum of all SS+DS plus triple-scattering signals, etc. It is clear that the SS model $\chi(n=2)$ fails to reproduce all peaks except the peak *D*. Scattering processes not less than the fifth order ($n \geq 4$) must be taken into account to fully describe the peaks of interest. The performed calculations, using MS formalism, confirm poor convergence of the path expansion near the threshold. Hence, using the FMS approach for calculating the spectra is necessary. Finally, in Fig. 1(d) a comparison between an experimental XANES spectrum and a simulated one is shown together with the *s* and *d* PDOS of Cd atom. A good agreement between experimental and theoretical spectra is achieved. It should be noticed that the vacuum level is used as a reference to the energy scale of the PDOS calculated by FEFF, which is typically several eV above the self consistently determined Fermi level. If one wants to use E-E_f energy scaling the present scale must be corrected using the Fermi level value given in one of *feff* output files.

B. Oxygen *K* edge—XAS

The experimental oxygen *K*-edge XANES spectra for CdO layers with different thickness and growth temperature are shown in Fig. 2(a). Here, the dipole-allowed transitions are from O 1*s* core state to unoccupied-states with *p* character above the Fermi level. No significant differences between the two spectra are observed. As was mentioned above, in case of a purely ionic Cd^{2+}-O^{2-} bonding, the 2*p* of oxygen states must be occupied and the transition $1s \rightarrow 2p$ should not be observed. However, this transition is clearly visible in the experimental (see Refs. 7 and 9) and calculated O *K*-edge XANES spectrum [see Fig. 2(c)]. Such an observation is coincident with results for L_3 Cd and suggests that the CdO films are not of purely ionic but rather of mixed character.

The results of a net charge given by FEFF (based on our input data) are as follows. For Cd atoms it is of +0.4, in contrast to an atomic configuration of s^2, and for the O atoms there is a net charge transfer of −0.4. These results show that the charge transfer to the O and Cd atoms is proportional to their valence, i.e., ± 2 with a factor of about 0.2. The charge transfer is roughly proportional to the oxidation state but also includes local screening charges. So, for instance, cadmium with a formal valence +2 has a net charge transfer of only about $+0.4e$.

As is well-known, highly ionic solids (>92% ionic) have the rocksalt structure and coordination number (CN) 6, whereas, highly covalent solids (0% ionic) show wurtzite or zinc blende (ZB) structure with CN 4. Calculated XANES

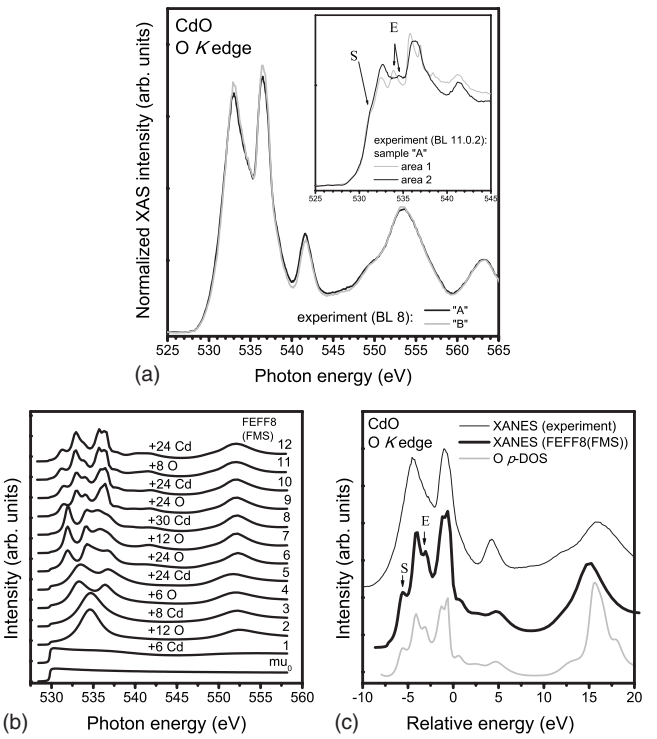

FIG. 2. (a) Experimental oxygen *K*-edge XANES spectra of CdO films (with different thickness and temperature growth). Data were collected in TFY detection mode. (b) Effect of increasing the number of scattering shells for the FMS calculation of the oxygen *K* edge of CdO film. Calculated signals were offset vertically. (c) Experimental (thin) and calculated (thick) CdO XANES spectra of *K* edge of O with oxygen *p* DOS (gray line). The data were vertically offset. E_F energy is −5.427 eV by FEFF8 code calculations. During calculation the Fermi level was shifted down (to place it in the midgap) by about 1.83 eV (see text).

spectrum for CdO with ZB structure does not reproduce the experimental one. So, we exclude the possibility of highly covalent bonding in investigated films. Our discussion indicates that investigated films are rather of dominant ionic type.

Calculated XANES spectra with increasing cluster size are shown in Fig. 2(b). Comparing XANES spectra versus cluster size it can be concluded that in the case of O *K* edge at least 171 atoms (cluster radius of about 7.8 Å, ten coordination shells) should be taken into account for calculations in order to obtain all the spectral features. Our primary restriction of the FMS cluster size in *feff.inp* file was ten coordination shells. From the calculated spectra as a function of the number of coordination shells (or cluster size) it could not be concluded that the calculated spectra converge for these cluster sizes since the XANES features are changing with every two shells. We added then, in turn, two extra shells changing the ancillary FEFF8 source code ("*nclusx*" is 175 by default) and finally set the FMS cluster size to about 8.5 Å (implying 202 atoms inside 12 coordination shells). Such calculations with our own input parameters take a much larger time (with Intel Core2 Quad CPU 2.66 GHz processor and 3 GB of RAM the differences in calculation time for FMS 7.8 and 8.5 Å are ~8 h versus ~20 h, re-

spectively) but after this procedure we can conclude that the results are converged in terms of the FMS cluster size.

We should emphasize that the atomic potentials, Fermi level and charge transfer are calculated self-consistently by FEFF code. Using the EXCHANGE card requires that the whole calculation be re-run with an energy shift added. The alternative and quicker method is to use the CORRECTIONS card which allows small changes in the Fermi energy to be made after the calculation is complete. The errors in FEFF's self-consistent Fermi level estimation are about 1–2 eV. This is particularly important for systems containing f electrons where the Fermi level placement is often incorrect. By shifting the calculated Fermi level by 1.83 eV a much better agreement with experiment is obtained for the absorption threshold, as the shoulder marked as "*S*" in Fig. 2(c) becomes visible in accordance with experimental data [see inset in Fig. 2(a)].

The energy positions of all significant experimental XANES peaks coincide with those in the XANES and PDOS calculated by FEFF8 [Fig. 2(c)] and reflect the O p unoccupied states. All the calculated peaks are well-resolved in the experimental spectrum except for two tiny features at about −5.6 eV and −3 eV [indicated by arrows and marked with letters "*S*" and "*E*" in Fig. 2(c), respectively] visible on PDOS which are leveled in the experimental spectrum due to the limited energy resolution and broadened due to the finite lifetime and, probably, film inhomogeneity. This supposition was confirmed by measuring the oxygen *K*-edge XANES spectra on beamline 11.0.2 (ALS) with energy resolution of about 0.07 eV and 300×300 μm^2 incident beam size [see the insert in Fig. 2(a)]. Here clearly browsed that both features *S* (shoulder on the absorption threshold) and *E* (an extra feature slightly above the first resonance) are coincident with the ones marked on theoretical XANES spectrum in Fig. 2(c). As the result of differences in setup, energy resolution and equipment on BL 8 versus BL 11.0.2 we were able to observe, on the last BL, in the energy region close the absorption threshold the distinct absorption profiles of the spectra collected from the different "areas" along the sample surface. Presented here spectra are the most characteristic for "as-grown" film where the dominating spectral profiles for different areas correspond to the area 2. We explain such differences in region of 530–535 eV as influence of native point defects on the electronic/local structure in CdO films and, perhaps, of film inhomogeneity. The obtained results will be published elsewhere.

The presented probing of unoccupied states with different orbital momentum and comparison of obtained results with calculated PDOS clearly show that minimum of the CB is assigned to O 2p hybridized with Cd 5s states.

C. Oxygen *K* edge—XES/RIXS

In order to probe the bulk-sensitive occupied VB electronic structure, near-threshold excitation x-ray emission spectra were recorded for CdO films for excitation energies at the O *K* absorption threshold. We point out that the XES experiments are unique since they can provide direct evidence to the band structure of a semiconductor, in particular

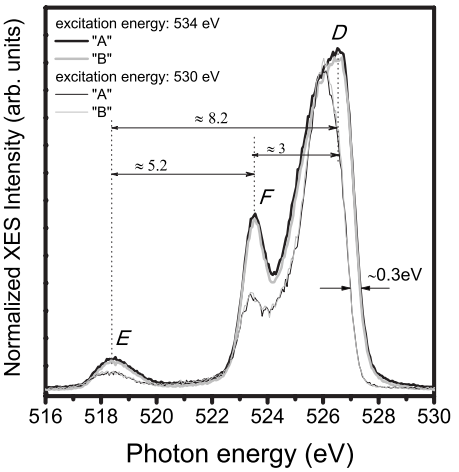

FIG. 3. Oxygen $2p\rightarrow1s$ XES spectra for CdO films with different thickness and growth temperature. The excitation energies were: 530 (thin black and gray lines) and 534 eV (thick black and gray lines).

whether a semiconductor has direct or indirect band gap, without further theoretical input.[21] In a XES experiment the band-gap type can be determined by observing the emission spectra as a function of excitation energy. In case of a direct energy gap material, emission at the highest energy is expected for an excitation energy in the vicinity of the absorption threshold (into the CB minimum, CBM). As the excitation energy increases the emission should shift to a lower energy. For indirect band-gap materials the opposite behavior is expected, i.e., a shift of the emission spectrum (namely, top of the VB maximum, VBM) to higher energy with increasing excitation energy. In another words, as the excitation energy increases, the probing transitions get closer, in $\boldsymbol{k}$ space, to the top of the VB. Our XES/RIXS data clearly show this tendency. Fig. 3 presents the O *K*-edge XES spectra recorded with two different excitation energies which demonstrate that increasing the excitation energy from 530 (excitation energies just below the absorption threshold) to 534 eV (slightly above the first resonance) shifts the top of the VB to higher energies at about 0.3 eV. This behavior results from a well-established $\boldsymbol{k}$-selectivity effect,[21] whereby restrictions on the intermediate state relaxation relatively enhances the emission at the $\boldsymbol{k}$ point of the CB minimum. Consequently, the selective appearance of a peak at 526 eV below the top of VB is a clear signature of an indirect band gap in CdO as opposed to a direct band-gap semiconductor which would have the opposite relative enhancement of spectral "weight" at the VBM.

As shown in Fig. 3, the XES spectra for the two films are very similar at the same excitation energies. Hence we performed RIXS measurements on only one of the samples. In the XES spectra shown in Fig. 3, three distinct features can be observed, labeled as *D*, *F*, and *E*. Features *D* and *F*, located at about 526 eV and at 523.5 eV, respectively, predominantly correspond to O 2p occupied states. The single-band shape *E* at about 518 eV is associated with transitions into the O 1s core hole from electrons in O 2p states hybridized with Cd 4d shallow electrons. The results presented here agree with the ones reported by Piper *et al.*[9] The separations

between the peak maxima are D-$E \sim 8.2$ eV, D-$F \sim 3$ eV, and F-$E \sim 5.2$ eV and agree well with those reported in a recent XPS study.[11] The theoretical bandwidth of the VB is the same as the experimental one (of about 5 eV) and agrees well with the value in Refs. 7 and 9.

As mentioned in the introduction, the size of CdO energy gap is still controversial. The experimental direct band gap values, accepted in literature, are around 2.3–2.4 eV.[4] The indirect band-gap size still remains ambiguous. The experimental values of indirect band gap represented in the literature vary from 0.55 and 0.84 eV (Refs. 22–24) to the higher ones of about 1.2 and 1.9 eV (Refs. 5 and 25–27). The same level of ambiguity exists in the reference data concerning the theoretical prediction of the indirect gap values, where the different ones are obtained using different approaches: linear combination of atomic orbitals [1.18 eV (Γ-L) and 1.12 eV (Γ-Σ)];[28] augmented plane wave [0.8 eV (Γ-L) and 1.2 eV (Γ-Σ) and 1.11 eV (Γ-L) and 0.95 eV (Γ-Σ)];[27,29] local-density approximation (1.7 eV);[30] GGA+U+Δ and HSE03 +GW (0.68 eV).[31] Up to now, we have not found any reports about the immediate evaluation of indirect gap values for CdO directly from combination of x-ray emission and absorption spectroscopy, except some attempts to indirectly estimate it.[7] To make up for this deficiency we performed RIXS measurements to probe transitions at different points in the Brillouin zone in the CdO film. In resonant excitation, the core electron is promoted to a bound state in the CB, so, the generated core hole recombines with the electrons from the higher electronic level (according to dipole transition rule), giving rise to the emission of a photon with the energy hv' less than the energy of incident radiation, hv. For comparison, nonresonant excitation occurs when the incoming radiation promotes a core electron to the continuum. When a core hole is created in this way, it could recombine through one of the several different decay paths. Since the core hole is refilled from the sample's high-energy free states, the decay and emission processes must be treated as the separate dipole transitions. It is in contrast to RIXS, where the events are concerned with each other and must be treated as a single scattering process.

The RIXS spectra (see Fig. 4) were recorded in 0.5 eV step through the threshold region up to the first absorption peak at about 533 eV, as indicated by arrows on the XAS spectrum [see Fig. 5(b)], and then for the resonances: 536.51, 541.7, and 553.5 eV. An elastic emission peak in the threshold-excited XES is used for correspondence with the XAS photon energy scale. The key experimental observation is the relative loss of intensity near the VB maximum and apparent shifts to lower energy as excitation energy is tuned closer to the CB minimum threshold (at about 528 eV). Nonlinearity of the VBM profile (see region 525–527 eV) in comparison with peak positioned at around 523.2 eV is clearly seen on the intensity map [see Fig. 6(a)].

To understand the energy shifts and RIXS line shape changes, a procedure for subtracting the residual "incoherent" fraction component of the RIXS spectra has been proposed and used for enhancing the band-structure effects of the coherent fraction component.[32] This involves using a high-energy excited spectrum well above threshold as a representative of the incoherent x-ray emission with $\boldsymbol{k}$ mixing

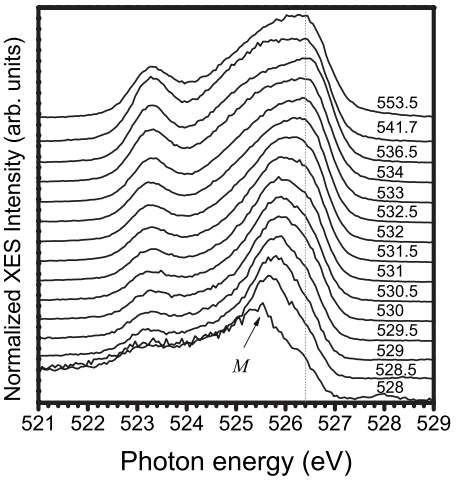

FIG. 4. Normalized to their maxima and vertically offset RIXS spectra of CdO film for excitation energies at the oxygen K-absorption threshold as indicated on the right side.

via intermediate state relaxations and scattering processes. This incoherent spectrum is then scaled and subtracted from the closer-to-threshold excited spectra with the restriction that remaining intensities must be positive. Below, we call such a procedure as a *standard* one. For indirect band-gap materials such as silicon and BeTe, this procedure has been applied with clean and understandable results.[33,34] However for CdO the leading energy shift of the VBM above threshold (see Fig. 3) is problematic for these data analysis procedure (namely for a few first excitation energies spectra) since even with different scaling either a negative intensity dip above the 527 eV VBM results from subtraction of a high-energy XES spectrum *or* subtraction has no effect on the spectra profile (an incoherent contribution is still there).

Hence there is a quandary that while there is 0% incoherent fraction between 527 and 527.5 eV in the 528 eV threshold spectrum, there is still clearly an incoherent shoulder from 526.2–527 eV extending above the 525.5 eV peak that one would like to subtract off (see Fig. 5). It is visible also after any type of subtraction taken for the estimation of pure coherent fraction. We propose that the CdO data set is showing a progressively varying *partial* $\boldsymbol{k}$ mixing of initial and final states near the threshold and thus a varying incoherent line shape. The failure to find a single representative experimental incoherent line shape results from an over-simplified approximation that breaks down, probably, for the very large 4 eV CB dispersion of CdO. The single incoherent line shape subtraction works well for Si and BeTe where the CB lowest branch dispersion is <1 eV (Refs. 33 and 34) and complete $\boldsymbol{k}$ mixing is easier even near the threshold. From this scenario, we then claim from Figs. 5 and 7 that the VB-CB gap in the XES-XAS threshold spectrum has no special meaning due to partial $\boldsymbol{k}$ mixing (it will be discussed later). Since the *standard* incoherent subtraction procedure could not result in completely removing the incoherent fraction and could not in full give a demonstration of the band structure of Γ_{15}-L and Γ_{15}-Σ branching effect [see Fig. 5(a)], we have decided, then, to how here, in parallel to the *standard* approach described above, how to arbitrarily enhance the excitation en-

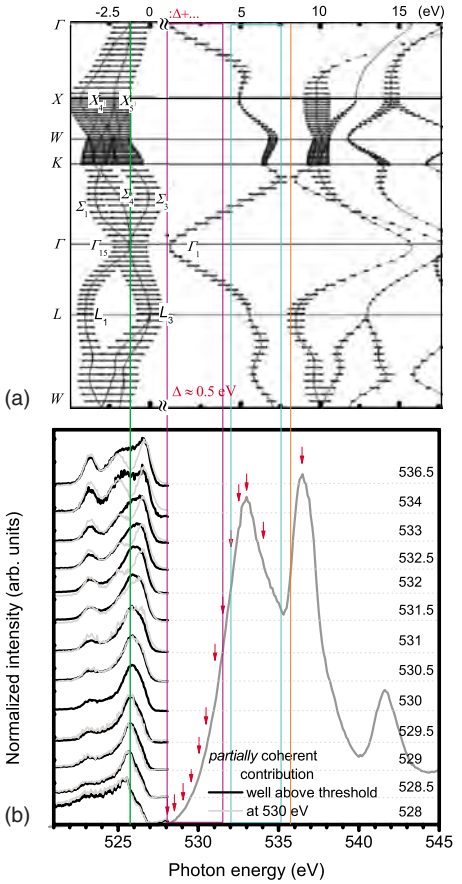

FIG. 5. (Color online) Energy-aligned comparison of (a) theoretical HSE03-*GW* band structure of CdO (Ref. 9) to (b) the *partially* coherent contribution of resonant XES spectra normalized to their maxima and vertically offset. To obtain partially coherent contribution two different approaches were applied: subtraction from RIXS data a XES spectrum well above the absorption threshold—black line, and XES spectrum at 530 eV—light gray line (see text for details). Additionally, the oxygen *K*-edge experimental XANES spectrum is shown on the right (dark gray line).

ergy line shape changes by subtracting off an intermediate XES spectrum at 530 eV. In Fig. 5(b) we present the resulting, *partially* coherent, emission spectra with comparison to the band structure [Fig. 5(a)] taken from Ref. 9. The *partially* coherent contributions corresponding to *standard* procedure are denoted by black lines, whereas light gray lines correspond to subtraction off an intermediate XES spectrum at 530 eV excitation energy (called here as an *intermediate*). In Fig. 6 we present intensity maps corresponding to *standard* and *intermediate* partially coherent fraction of XES along with RIXS for a better visualization of band dispersion branches away from the Γ_{15} point [see Fig. 6(a)]. To align the calculated band structure with respect to the experimental data we match the VB Γ_{15} high-symmetry point with the VBM of XES corresponding to excitation energy at 528.5 eV, so, the CBM has been shifted from the theoretical value of 1.9 eV to the optical experimental value at about 2.4 eV. The estimated direct band gap value for CdO *A* and *B* films, from our own optical absorption measurements, by an extrapolation of the square of the absorption coefficient comes

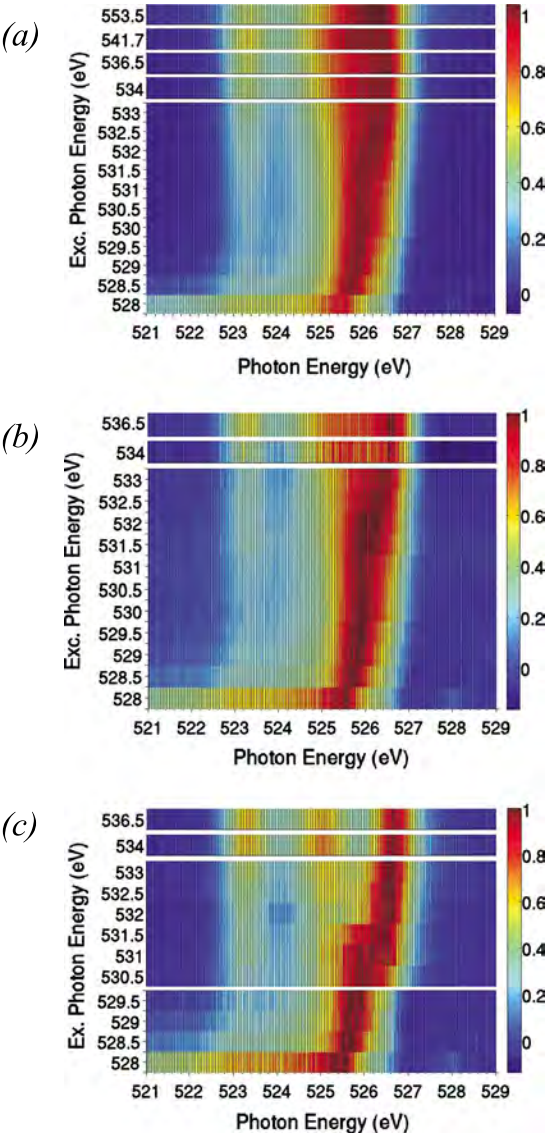

FIG. 6. (Color online) (a) Intensity maps of normalized RIXS and partially coherent fractions of XES corresponding to (b) *standard* and (c) *intermediate* approaches (see text for details). *Intermediate* procedure works well for visualization of branching dispersion of occupied states.

to ~2.4 eV. Qualitatively, the aligned band structure agrees quite well with our results. This comparison highlights the low-energy and high-energy dispersions of the VB intensity with a good correspondence to the *X* and *L* high-symmetry points that lie at about 0.6 eV below and at about 1.0 eV above the Γ-point Γ_{15} energy. In addition, the band midway of the Γ-*K* region has a similar higher energy dispersion as the *L* point that theoretically gives a near identical indirect band-gap value. Note that the coherent emission from these three $\boldsymbol{k}$ points (*X*, *L*, and Γ-*K*) all coincidently exists for similar CB energies of about 4 eV above the Γ_1-point threshold energy. Thus, the *X*-point lower energy branch experimentally develops and reaches maximum simultaneously with the indistinguishable *L* and Γ-*K* higher energy branches.

The Cd 5*s* orbital with even symmetry and the O 2*p* orbital with odd symmetry cannot mix at the Γ point, so, the

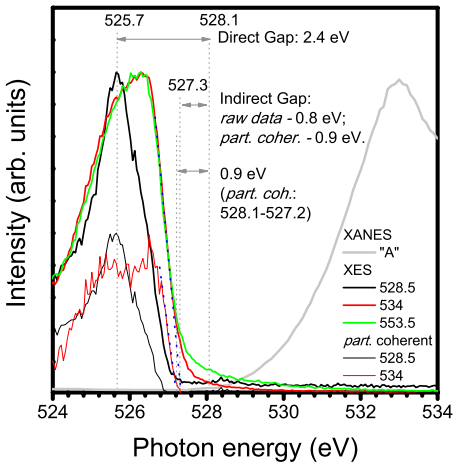

FIG. 7. (Color online) Zoomed threshold region of oxygen $2p \rightarrow 1s$ XES and $1s \rightarrow 2p$ XAS spectra for CdO film with quantitative identification of direct and indirect band gaps. The excitation energies were 528.5 (thick black), 534 (thick red), and 553.5 (thick green) eV. Black and red thin lines correspond to partially coherent fraction (*standard*): 528.5 and 534 eV, respectively (see text for details, curves of the smaller intensity). XES energy scale was aligned to XAS one by using of elastic peak on emission spectra.

translation symmetry constraints are such that the Cd $5p$-O $2p$ interaction is fully antibonding.[35] Taking this into account and comparing our PDOS distribution (see Figs. 1 and 2) with the presented band structure [Fig. 5(a)] we are able to conclude that the orbital character of the lowest energy CB branch is mostly of Cd $5s$-O $2p$ σ^*. As is well known, the VB upper bands have predominantly O $2p$ character.

To extract accurate emission peak energy, the energy positions of the different lines contributing to the structures in the partially coherent fractions (contributions corresponding to the standard one were used for this purpose) were determined by assuming Gaussian line shapes. In Fig. 5(b) XAS region is conditionally divided into three parts. The first one includes CBM and the absorption threshold (magenta contour, at about 528–531.5 eV), the second—the area around the first resonance (blue contour, at about 532–535 eV) and the third—the second resonance and above region (starting from the orange line, at about 535.8 eV). In the first part ($h\nu$=528−531.5 eV), we begin with the profiles almost entirely dominated by the peak at about 525.7 eV. According to the band structure the CBM is located at the Γ point (Γ_1 energy) in the Brillouin zone. Hence, the peak at about 1.25 eV below the VBM (at 525.7 eV on photon energy scale) is due to states at the Γ points (Γ_{15} energy) which have p oxygen local symmetry. Consequently, for excitation energy close to the CBM, the emission peak is due to a dominant contribution from the Γ point (Γ_{15} energy). When the excitation energy increases up to 530 eV an additional emission contribution at 526.6 eV becomes fully visible (a pronounced shoulder on the right side). It arises from Γ-L and Γ-K regions (branching off from the Γ_{15} point). Progressive increase of the excitation energy (up to 531.5 eV) enlarges the shoulder contribution and indicates the emission moving along Γ_{15}-L_3 and Γ_{15}-Σ_3 branches in higher energy direction. The lower energy tail (from 525.7 to about 524 eV) and peak at around 523.2 eV are due to contributions from the Γ-L, Γ-K, and Γ-X regions with a major contribution from the X point for the last peak. The peak position at 523.2 eV agrees well with the position presented by McGuinness *et al.*[7] for polycrystalline CdO but it is shifted for about −1 eV in comparison with single crystal of CdO.[9] It should be noticed that for excitation energies not matching high symmetry points there is a certain ambiguity because generally more than one crystal momentum can be reached at each excitation energy.

In the second region (blue contour in Fig. 5) differences in partially coherent contribution (*standard* vs *intermediate*) are significant and describe well the VB branches dispersion [see Figs. 5(b), 6(b), and 6(c)]. When excitation energy increases (532–533 eV) the main emission peak at around 526 eV starts to be more asymmetric and is split into three subpeaks at about 526.6, 526, and 525.2 eV. The peak at 526.6 eV is still from the Γ-K (close to Σ_3 energy) and Γ-L (close to L_3 energy) regions. The next feature at 526 eV arises from the Γ-K (close to Σ_4 energy) and Γ-X-W regions. The peak at 525.2 eV is due to Γ-X and X-W regions (mainly around the X point). The resonance at around 523.2 eV is associated with the Γ-K (close to Σ_1 energy), Γ-L (close to L_1 energy) regions, and Γ-X-W area close to the X point.

By inspecting spectra at $h\nu$=534 eV we notice the same contribution as above for emission at 526.6 eV. The feature at about 526 eV originates from the K point and L-W region. The peak at around 525.2 eV is due to the X-W-K, L-W, and Γ-K regions (close to W and K points).

Generally, further increasing of excitation energy results in transitions from higher energy branches with lower band dispersion at this excitation energy, what increases the contribution of appropriate emission peaks. At an excitation energy of 536.5 eV the regions L-W and Γ-K are predominantly excited. So, peaks at around 526.6 eV (L_3 and Σ_3 energy branches) and at around 523.2 eV (close to L_1, Σ_1, and X_4 energy branches) are more pronounced for $h\nu$ =536.5 eV than for other excitation energy. Contribution into the emission peak at 526 eV is also from the W-L and Γ-K (close to the K point) regions.

D. Estimation of band-gap values

In Fig. 7 the overlapping of selected XES and XAS spectra (with the excitation energies equal to 528.5, 534, and 553.5 eV) in photon energy scale is presented. Two curves corresponding to partially coherent contributions (standard ones) are added to the plot (at 528.5 and 534 eV of excitation energy, curves of the smaller intensity) for more precise estimation of energy gap. Starting from the excitation energy of 534 eV the edge of VB remains at the same energy and only the high energy tail increases its intensity. It should be noticed that the VB maximum (labeled as “M” in Fig. 4) movement occurs without any constant energy separation from the elastic peak position when the excitation energy increases. This suggests that the VBM for excitation energy of 528 eV cannot be associated with a constant (Raman-type) loss feature. To be firmly convinced, we assume the 528.5 eV excitation energy spectrum to be a determinative one during

our estimation of band-gap value. Taking into account that the CB minimum lies at 528.1 eV (point where absorption starts, obtained by taking the first nonzero values of the XAS spectrum first derivative), and the maximum of XES spectrum with the lowest excitation energy (528.5 eV) lies at 525.7 eV, we can evaluate the band-gap value to be 2.4 eV (Γ_1-Γ_{15} gap on the band structure). This is in good agreement with the direct band gap value presented in the literature and coincident with our own optical results.

Next, the difference between the CBM and the top of VB (at about 527.2 eV close to the L point) with the highest excitation energy is equal to about 0.9 eV which is in quite good agreement with the reported indirect band gap of 0.84 eV.[24] Moreover, as is well known, the procedure of the indirect band-gap value estimation in case of thin CdO films by means of optical absorption spectra faces essential difficulties in view of weak signal and influence of Fabry-Pérot oscillations on the pre- and near-edge region. In order to directly measure the indirect gap of CdO by optical absorption we grew, then, a thick CdO film (0.6 μm) so the indirect gap absorption is more significant. Electrical property of this thick CdO film is comparable to the thin CdO we studied here. Linear extrapolation of the square root of the absorption coefficient gave a value of indirect band gap at about 0.95 eV which agrees well with our results discussed above.

Thus, combination of Figs. 5 and 7 allows us to conclude that for investigated CdO thin films—(i) the direct energy gap at the Γ point is $\sim$2.4 eV, (ii) an indirect gap of $\sim$0.9 eV which implies dispersion along Γ-L and Γ-K, and (iii) lower energy dispersion along Γ-X. Furthermore, the overall theoretical VB bandwidth is in good agreement with the lower energy XES peak at about 518 eV and overall 4–5 eV band width. Such clear and distinct indirect band gap and valence band dispersion signatures in CdO RIXS were not observed in previous x-ray emission studies,[9] in part, because of the worse resolution and since the threshold excitation region down to 528 eV was not probed.

IV. CONCLUSIONS

In this work we present a detail interpretation of x-ray absorption near edge structure at the K and L_3 edges of oxygen and cadmium in CdO film within the *ab initio* FMS formalism (FEFF8 code). Based on RSMS theory we were able to interpret the experimental spectra in terms of local geometrical and electronic structures. Calculated near-edge structure for cation and anion x-ray absorption edges represents a good coincidence with experimental one. Not purely ionic bonding in CdO is identified. Calculated PDOS describes well all features corresponding to unoccupied states of investigated films and allows to conclude that the orbital character of the lowest energy of the CB is mostly Cd 5s-O 2p σ^*.

Presented RIXS CdO data set is showing a progressively varying *partial* $\boldsymbol{k}$ mixing of initial and final states near the threshold and thus a varying incoherent line shape. Overlapping of XAS spectrum with RIXS ones makes possible to estimate both direct $\sim$2.4 eV and indirect $\sim$0.9 eV band-gap values. The obtained results are consistent with the theoretical/experimental ones presented in the literature and our own optical absorption results.

ACKNOWLEDGMENTS

The authors wish to thank the staff of the ALS for their excellent support (especially W. Yang, W.C. Stolte, and T. Tyliszczak). This work was performed at the Advanced Light Source, which is supported by DOE (Grant No. DE-AC03-76SF00098). Work performed by K. M. Yu, D. Speaks, and W. Walukiewicz was supported by the Director, Office of Science, Office of Basic Energy Sciences, Materials Sciences and Engineering Division, of the U.S. Department of Energy under Contract No. DE-AC02-05CH11231. The authors wish to thank also group of C. Heske (UNLV) for experimental support and useful discussions.

[1] Q. Zhou, Z. Ji, B. Hu, C. Chen, L. Zhao, and C. Wang, Mater. Lett. **61**, 531 (2007).
[2] L. F. J. Piper, L. Colakerol, P. D. C. King, A. Schleife, J. Zuniga-Perez, P.-A. Glans, T. Learmonth, A. Federov, T. D. Veal, F. Fuchs, V. Munoz-Sanjose, F. Bechstedt, C. F. McConville, and K. E. Smith, Phys. Rev. B **78**, 165127 (2008).
[3] W. Walukiewicz, J. W. Ager III, K. M. Yu, Z. Liliental-Weber, J. Wu, S. X. Li, R. E. Jones, and J. D. Denlinger, J. Phys. D **39**, R83 (2006).
[4] R. Blachnik *et al.*, in *Semiconductors*, Landolt-Börstein, New Series, Group III Vol. 41B, edited by U. Rössler, Supplement to Vols. III/17b, 22a, Revised and Updated edition (Springer, Berlin, 1999), p. 312.
[5] M. Altwein, H. Finkenrath, C. Konak, J. Stuke, and G. Zimmerer, Phys. Status Solidi **29**, 203 (1968).
[6] E. Burstein, Phys. Rev. **93**, 632 (1954).
[7] C. McGuinness, C. B. Stagarescu, P. J. Ryan, J. E. Downes, D. Fu, K. E. Smith, and R. G. Egdell, Phys. Rev. B **68**, 165104 (2003).
[8] Y. Dou, T. Fishlock, R. G. Egdell, D. S. L. Law, and G. Beamson, Phys. Rev. B **55**, R13381 (1997).
[9] L. F. J. Piper, A. DeMasi, K. E. Smith, A. Schleife, F. Fuchs, F. Bechstedt, J. Zuniga-Perez, and V. Munoz-Sanjose, Phys. Rev. B **77**, 125204 (2008).
[10] In the *GW* approximation to the many-body perturbation theory, the self-energy $\sigma(E)$ is approximated as the product of the one-electron Green's function G and the dynamically screened Coulomb interaction W.
[11] P. D. C. King, T. D. Veal, A. Schleife, J. Zuniga-Perez, B. Martel, P. H. Jefferson, F. Fuchs, V. Munoz-Sanjose, F. Bechstedt, and C. F. McConville, Phys. Rev. B **79**, 205205 (2009).
[12] A. L. Ankudinov, B. Ravel, J. J. Rehr, and S. D. Conradson, Phys. Rev. B **58**, 7565 (1998).
[13] J. J. Rehr and R. C. Albers, Rev. Mod. Phys. **72**, 621 (2000).
[14] H. Modrow, S. Bucher, J. J. Rehr, and A. L. Ankudinov, Phys. Rev. B **67**, 035123 (2003).

[15] B. Ravel, J. Alloys Compd. **401**, 118 (2005).
[16] J. L. Beeby, Proc. R. Soc. London, Ser. A **302**, 113 (1967).
[17] P. Lloyd and P. Smith, Adv. Phys. **21**, 69 (1972).
[18] http://leonardo.phys.washington.edu/feff/html/documentation.html
[19] J. J. Rehr, J. Mustre de Leon, S. I. Zabinsky, and R. C. Albers, J. Am. Chem. Soc. **113**, 5135 (1991).
[20] http://www.esrf.eu/UsersAndScience/Experiments/CRG/BM30B/Mendeleev/48-Cd.html
[21] S. Eisebitt, J. Luning, J.-E. Rubensson, and W. Eberhardt, Phys. Status Solidi B **215**, 803 (1999).
[22] O. Madelung, M. Schulz, and H. Weiss, *Semiconductors: Physics of II-VI and I-VII Compounds*, Landolt-Bornstein, New Series, Group III Vol. 17b (Springer, Berlin, 1982).
[23] H. Köhler, Solid State Commun. **11**, 1687 (1972).
[24] F. P. Koffyberg, Phys. Rev. B **13**, 4470 (1976).
[25] J. Kocka and C. Konak, Phys. Status Solidi B **43**, 731 (1971).
[26] A. A. Dakhel and F. Z. Henari, Cryst. Res. Technol. **38**, 979 (2003).
[27] K. Maschke and U. Rössler, Phys. Status Solidi **28**, 577 (1968).
[28] A. Breeze and P. G. Perkins, Solid State Commun. **13**, 1031 (1973).
[29] S. Tewari, Solid State Commun. **12**, 437 (1973).
[30] D. Vogel, P. Kruger, and J. Pollmann, Phys. Rev. B **54**, 5495 (1996).
[31] A. Schleife, C. Rödl, F. Fuchs, J. Furthmüller, and F. Bechstedt, Phys. Rev. B **80**, 035112 (2009).
[32] J. Lüning, J.-E. Rubensson, C. Ellmers, S. Eisebitt, and W. Eberhardt, Phys. Rev. B **56**, 13147 (1997).
[33] S. Eisebitt, J. Lüning, J.-E. Rubensson, A. Settels, P. H. Dederichs, W. Eberhardt, S. N. Patitsas, and T. Tiedje, J. Electron Spectrosc. Relat. Phenom. **93**, 245 (1998).
[34] D. Eich, O. Fuchs, U. Groh, L. Weinhardt, R. Fink, E. Umbach, C. Heske, A. Fleszar, W. Hanke, E. K. U. Gross, C. Bostedt, T. v. Buuren, N. Franco, L. J. Terminello, M. Keim, G. Reuscher, H. Lugauer, and A. Waag, Phys. Rev. B **73**, 115212 (2006).
[35] J. L. G. Fierro, *Metal Oxides: Chemistry and Applications* (Taylor & Francis, London, 2006).

DISCLAIMER